

Simulation of multiply scattered elastic waves with 3D wave-equation and radiative transfer equation for displacements and their gradients

- Mirko Bracale¹: mirko.bracale@univ-grenoble-alpes.fr
- Ludovic Margerin²: ludovic.margerin@irap.omp.eu
- Romain Brossier¹: romain.brossier@univ-grenoble-alpes.fr
- Michel Campillo¹: michel.campillo@univ-grenoble-alpes.fr

¹ISTerre, Université Grenoble Alpes, CNRS, Université Savoie Mont Blanc, IRD, Université Gustave Eiffel, Grenoble, France

²Institut de recherche en astrophysique et planéologie (IRAP/OMP), CNRS, CNES, Université Toulouse III - Paul Sabatier, Toulouse, France

This is a non-peer-reviewed preprint submitted to EarthArXiv.

Simulation of multiply scattered elastic waves with 3D wave-equation and radiative transfer equation for displacements and their gradients

Mirko Bracale¹, Ludovic Margerin², Romain Brossier¹,
Michel Campillo¹

¹ISTerre, Université Grenoble Alpes, CNRS, Université Savoie Mont Blanc,
IRD, Université Gustave Eiffel, Grenoble, France

²Institut de recherche en astrophysique et planétologie (IRAP/OMP),
CNRS, CNES, Université Toulouse III - Paul Sabatier, Toulouse, France

April 18, 2025

Corresponding author: Mirko Bracale: mirko.bracale@univ-grenoble-alpes.fr

Abstract

In this study, we investigate the behavior of seismic waves in a highly scattering medium using numerical simulations of the full wavefield, based on Spectral Element Method solutions of the wave equation. The simulated

3D elastic medium was designed with Von Kármán-correlated heterogeneity, providing a realistic representation of the complexities present in natural seismic environments. We analyzed three distinct cases, each characterized by increasing levels of heterogeneity fluctuation, with standard deviations ranging from 10% to 25%, both at depth and at the free surface, allowing us to compare the behavior of seismic waves under varying conditions. We validated the consistency between theoretical predictions of the scattering theory and simulations of the elastic wave equation using Spectral Elements Methods. We compared the results in terms of the mean free path, long-term energy evolution, and the partitioning of energy between compressional and shear modes. For the latter, the validation was supported by numerical simulations of the elastic Radiative Transfer Equation. We show that under specific conditions, existing Spectral Elements simulation codes can effectively replicate wave propagation in a highly scattering medium. This implies that a greater part of the waveform, namely the late envelopes, could be employed in inversion processes, thus opening up new possibilities in the realm of inversion studies. Furthermore, we investigated the energy envelope of the displacement wavefield and its gradient to demonstrate how the analysis of the rotational field can provide additional insights into the source mechanism, the propagation direction and the polarization of seismic waves.

Keywords: Wave propagation, Computational seismology, Theoretical seismology, Wave scattering and diffraction.

1 Introduction

Simulating wave propagation means solving the wave equation with numerical methods, knowing the properties of the propagation medium and the seismic source. The accuracy of seismic numerical simulations in reproducing wave propagation in homogeneous layered media has been extensively studied in the past, using various methods to solve the wave equation (Virieux and Operto, 2009; Igel, 2017; Trinh et al., 2019). The propagating medium is discretized into elements to which the elastic properties, typically in the form of P-wave and S-wave propagation velocities and density, are assigned, uniform within each element. The reliability of the synthetic seismograms computed is limited to a defined range of frequencies, depending on the method and the parameters used to solve the wave equation (Igel, 2017).

In this study, we use the spectral element methods (SEM), implemented in the SEM46 code (Trinh et al., 2019), which takes its original formulation in the reference SEM literature (Komatitsch and Vilotte, 1998; Komatitsch and Tromp, 1999). This numerical method has demonstrated good ratio between accuracy and computing time using 4th order polynomial interpolation within elements. This level of accuracy has been validated in simple models, where comparisons with analytical and other numerical solutions are feasible, focusing on ballistic waves such as direct, reflected, refracted, surface waves (Komatitsch and Vilotte, 1998; Komatitsch and Tromp, 1999). Introducing small scale highly heterogeneous medium presents however significant challenges due to the complexity of

multiple scattering phenomena, complicating the reliability assessment of such simulations.

The primary objective of this study is to test the reliability of numerical simulations in highly heterogeneous media over extended time periods. This issue has been addressed in the past by several studies (Frankel and Clayton, 1986; Pham et al., 2009; Nakahara and Yoshimoto, 2011; Obermann et al., 2016; Emoto and Sato, 2018; Celorio et al., 2022). To evaluate the reliability, it is necessary to compare the results of numerical simulations with the theoretical predictions of scattering theory. In this study, we focused on three key aspects: the scattering mean free path, the transition between multiple scattering and diffusion regimes, and the evolution of the energy partition ratio over time.

A significant challenge lies in the fundamental differences between the approaches used in scattering theory and those employed to describe wave propagation via the wave equation. The wave equation provides a deterministic solution for ground motion at specific observation points, retaining both phase and amplitude information of the propagating signal. Scattering theory, on the other hand, adopts a statistical framework. In particular, scattering theory generally requires that the scattering properties of the medium are uniform throughout and that the elastic parameters are spatially correlated with a given autocorrelation function (ACF) (Sato and Fehler, 2012). To compare the two simulations, such a medium was also considered when solving the wave equation.

Central to scattering theory is the Radiative Transfer Equation (RTE), which models energy density mode conversion and propagation in a heterogeneous medium

(Weaver, 1990; Ryzhik et al., 1996; Turner and Weaver, 1994; Margerin, 2005).

The RTE provides a solution for a statistically homogeneous medium over a defined propagation distance, inherently excluding seismic phase information. Generally, the solution offered by the RTE is averaged over a specified distance, yielding the mean energy intensity observed at that distance for a medium with statistically defined elastic properties.

While intensity can, in principle, be derived from ground motion obtained via wave equation simulations, it cannot be directly compared with predictions from scattering theory, as it constitutes a local measure. Consequently, special methodologies are required to compare the outputs from these two approaches called "ensemble average" and "spatial average".

The first method involves running multiple simulations of the wave equation with the same scattering characteristics of the medium but different configurations of heterogeneities (referred to as realizations). The average of the results across these different realizations is then used to extract the statistical characteristics of the wavefield. While this approach is more accurate, as it accounts for different media that share the same statistical properties as described by theory, it is computationally expensive, particularly for three-dimensional simulations, as extensively discussed in this work.

In this study, we employed the second method, the spatial average, which requires only a single realization, provided that the conditions of complete isotropy and uniform statistical properties are met. Receivers must be symmetrically distributed around the source, and averages are calculated at specific distances. This

approach assumes that wave paths are independent, meaning that waves arriving at different receivers primarily interact with distinct heterogeneities. This condition is not fully satisfied but can be considered valid if the receivers are sufficiently spaced. The only issue arises because heterogeneities located near the source generate a correlation between the signals observed at all positions (Shapiro, 1999). In this work, we focus on the transport regime in which the scattering mean free path l is much greater than the wavelength λ . In this case, the contribution of long-range correlations of order l/λ can be considered negligible.

In this work, three different case study were considered with increasing strengths of heterogeneities: 10%, 17%, and 25%, in both full-space and half-space media, using different types of source mechanisms. In all these cases, the medium features realistic heterogeneities with a Von Kármán correlation and a correlation length of 320m. For each case, we perform extensive comparisons between the outputs of the numerical simulations and the predictions of RTE regarding attenuation of the coherent waves, the onset of diffusion and the partition of energy between different wave modes.

We would like to draw the attention of the reader to the fact that while RTE is well established in the full space case, the half-space and waveguide geometries have been the topic of intense research in the last twenty years (Tregoures and van Tiggelen, 2002; Zeng, 2006; Maeda et al., 2008; Margerin et al., 2019; de Hoop et al., 2022; Xu et al., 2022). From a practical perspective the key difference between the different approaches lies in the formulation of the coupling between surface and body waves. (Tregoures and van Tiggelen (2002); de Hoop et al. (2022))

employ an eigenmode decomposition of the wavefield while [Maeda et al. \(2008\)](#); [Margerin et al. \(2019\)](#); [Xu et al. \(2022\)](#) use a more straightforward ray theoretical representation of the body waves. In the latter formulations, our numerical approach offers a unique opportunity to estimate the coupling terms between body and surface waves based on the wave equation.

This article is organized into two main parts. In the first part, we perform a reliability assessment, comparing results from SEM simulations with those derived from scattering theory in both full-space and half-space media. It should be noted that we have not considered the possibility of a rough topography, which would also be locally the source of significant conversions between propagation modes (e.g. [Sánchez-Sesma and Campillo, 1991](#); [Rodgers et al., 2010](#)).

In the second part, we revisit these cases to investigate the energy evolution of the three components of the displacement wavefield and its gradients in the form of normal strain, and rotation generated by an isotropic source mechanism.

2 Simulations in a Full Space Medium

In this section, we discuss the numerical simulations conducted in a full-space medium for increasing levels of heterogeneity: $\epsilon = 10\%$ and $\epsilon = 25\%$. These two cases are considered to be the most significant as they represent the limits within which we tested our models. The full simulation parameters are listed in the Supplementary Material, Table S1. In Fig. [1](#)(a), we show the source-receiver configuration used for three sets of receivers on concentric spheres. 2521 receivers

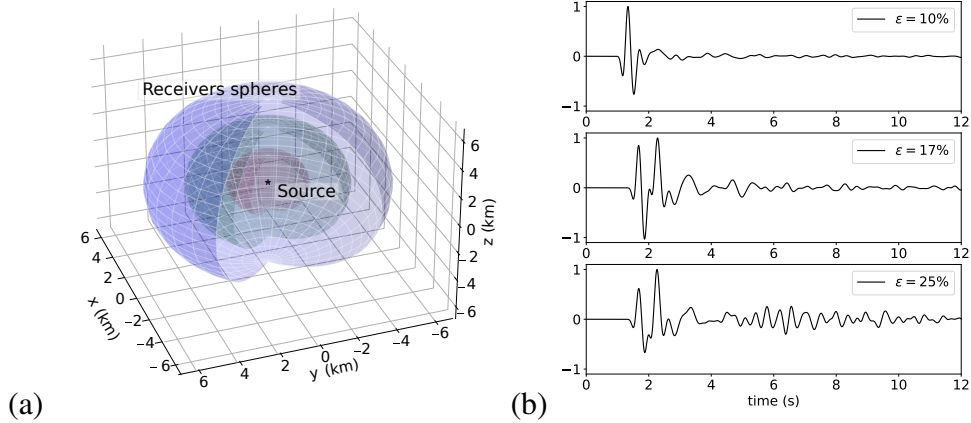


Figure 1: (a) Source-receiver configuration. 2521 receivers have been deployed on each sphere. (b) Seismograms of displacement along the radial direction at a distance of 2 km from the source, for increasing strength of heterogeneity.

were placed on 36 concentric spheres, with a minimum radius of 2 km, increasing by 0.5 km. The source, characterized by an isotropic moment tensor, was positioned at the center. On these spheres, the receivers' axes are rotated to obtain a radial component directed towards the source and transverse components tangent to the spheres. By averaging observations from these symmetrically distributed observation points, we provide an estimation of the average wave behavior, minimizing the influence of random fluctuations.

Fig. 1 (b) shows the seismogram of radial displacements recorded at 2 km distance from the source in three cases of increasing heterogeneity standard deviation, ϵ . It is possible to observe how, with increasing ϵ , scattering attenuates ballistic arrivals and transfers the coherent energy to the coda.

2.1 Mean free path computation

In Fig. 2(a) and Fig. 3(a), the coherent field is shown at distances ranging from 2 to 14 km from the source in the two cases with $\epsilon = 10\%$ and $\epsilon = 25\%$. It is evident that as one moves away from the source, the interaction with heterogeneities increases, and in some cases, even spatial averaging is unable to remove the fluctuations. In the first case study, the coherent field remains well preserved even at a distance of 14 km from the source. Conversely, in the second case study, because of the strong scattering even at 5 km distance, the coherent part of the signal can be extracted, but the fluctuations are not adequately suppressed. At greater distances, these fluctuations significantly affect the signal and its spectrum. To analyze quantitatively this phenomenon, we performed an analysis in which we considered the spatial average at two reference distances and calculated the ratio between the standard deviation of the coda and that of the ballistic arrivals. It is expected that if the spatial average effectively removes the fluctuations, this ratio should be close to zero. In the simulation with $\epsilon = 10\%$ percent, at distances of 4 km and 8 km, the ratios obtained were 0.010 and 0.012, respectively. In the second simulation, where $\epsilon = 25\%$, the ratios obtained were 0.176 and 0.424 at the same distances. This indicates that, despite the spatial averaging, a significant amount of energy remains in the coda in the second case.

The results obtained from the numerical simulations were then compared with the theoretical results given by [Sato and Fehler \(2012\)](#).

The results, shown in Fig. 2(b), where $\epsilon = 10\%$, indicate that our findings align with theoretical expectations, at least within the frequency range of 1.7 Hz

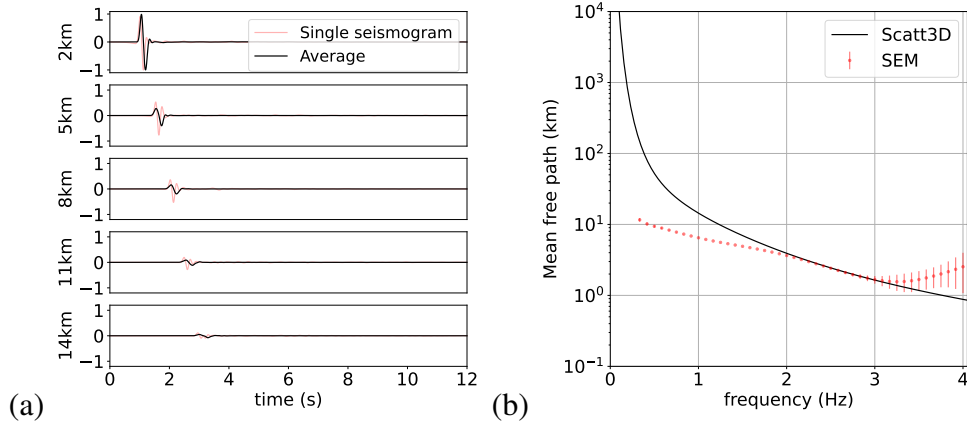


Figure 2: Simulation with $\epsilon = 10\%$. (a) Coherent field, obtained by averaging the radial component of the displacement at increasing distance from the center. (b) Comparison between the mean free path computed with SEM and RTE. A good agreement is found between about 1.7Hz and 3.0Hz.

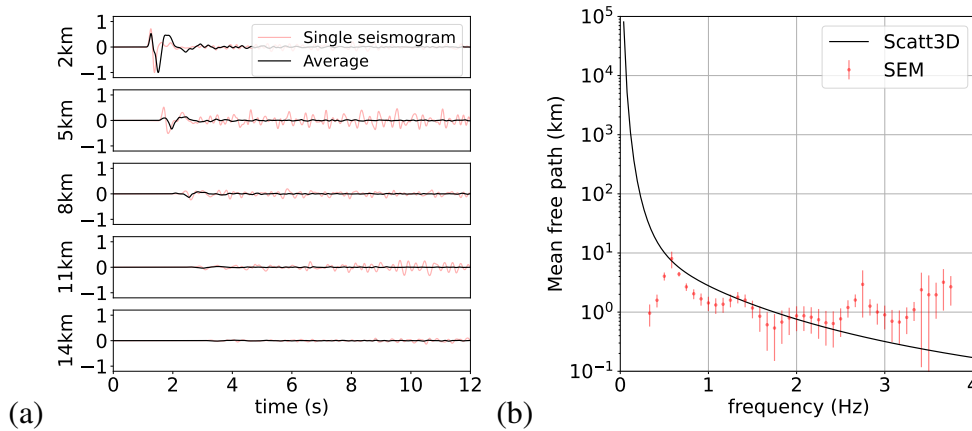


Figure 3: Simulation with $\epsilon = 25\%$. (a) Coherent field. (b) Comparison between the mean free path computed with SEM and RTE. The frequency dependence of the is well captured between about 0.5 and 2.5Hz.

to 3 Hz. These boundaries are set by the simulation configuration. The lower limit is due to the fact that when the scattering mean free path becomes comparable to the medium size, wave attenuation is too weak to be measured effectively. The upper limit arises from the issue that if the scattering mean free path is too small relative to receiver spacing, signal decay occurs too rapidly to be measured.

This analysis allows us to assert that frequencies within this range are reliable. However, it is important to note that frequencies outside of this range may also be well represented. The accuracy of this measurement could be influenced solely by the method used. In the following analyses, good agreement between SEM and RTE has been found in the range of frequency between 0.9Hz and 3.0Hz.

In the case $\epsilon = 25\%$, Fig. 3 illustrates that the computation of the mean free path matches the expectations only for a limited range of frequency. This is due mainly to the fact that the fluctuations are not fully removed by the averaging process because much more scattering is produced (see Fig. 3 a).

2.2 Transition from multiple scattering to diffusion

As the time lapse increases, it is expected that seismic waves interact with more heterogeneities, passing from the multiple scattering regime to the diffusive regime. This regime is characterized by the fact that the energy flux becomes weakly anisotropic and the energy density follows the diffusion equation. The solution of this equation for a three-dimensional medium is the following:

$$E(\mathbf{r}, t) = \frac{S_0}{(4\pi Dt)^{3/2}} e^{-\frac{r^2}{4Dt}}, \quad (1)$$

where S_0 is the source term and D is the diffusivity. Close to the source, for small r , the decay of the energy with time is proportional to the factor $t^{-3/2}$. A characteristic parameter of this equation is the characteristic time or Thouless time, defined as $\tau_D = r^2/D$, which quantifies the rise time of the energy envelope. The comparison between the diffusivity constant, in the 10% case, obtained in the SEM simulations (3.0km²/s) and that obtained from the RTE (3.2km²/s) was found to be consistent. The fit is shown in the Supplementary Material, Fig. S2.

The energy decay observed at distance of 4.5 km in the two cases (a), $\epsilon = 10\%$ and (b), $\epsilon = 25\%$ is shown in Fig. 4.

The energy has been averaged considering the receivers located at that distance. In the first case, a good fit is visible starting at about 12 seconds, which corresponds to $\tau_D = 6.8$ seconds ($D = 3 \text{ km}^2/\text{s}$) while in the second case a good fit is achieved already at 8 seconds $\tau_D = 1.3$ seconds ($D = 16 \text{ km}^2/\text{s}$). This difference arises because scattering anisotropy, mean free time, and consequently diffusivity depend on the heterogeneity strength ϵ , which differs significantly between the two cases. Refer to the Supplementary Material, Fig. S3, for the plots of the mean free times.

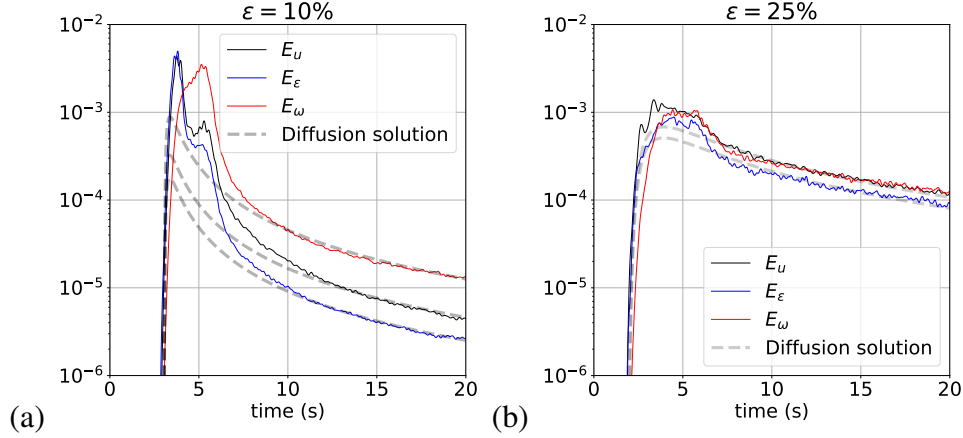


Figure 4: Comparison between energies derived from SEM simulations and predictions of the diffusion approximation. The displacement energy $E_u = u_x^2 + u_y^2 + u_z^2$, rotation energy $E_\omega = \omega_x^2 + \omega_y^2 + \omega_z^2$ and strain energy $E_\epsilon = \epsilon_{xx}^2 + \epsilon_{yy}^2 + \epsilon_{zz}^2$ are shown for two levels of heterogeneity. Computations correspond to source to receiver distance of 4.5km. The diffusion regime starts at about 12 seconds in the $\epsilon = 10\%$ simulation (a) and at about 8 seconds in the $\epsilon = 25\%$ simulation (b)

2.3 Energy partition ratio

The interaction of waves with heterogeneities generates conversion between longitudinal energy E_p and shear energy E_s . To compute these two energies we used the normal strain, ϵ_{ii} , and rotations, ω_i .

The calculation of the P and S energy is simplified by the fact that the S field has null divergence while the P field is irrotational. This condition allows us to define the energies in the following way:

$$E_P = (\lambda + \mu)(\nabla \cdot \mathbf{u}(t))^2 = (\lambda + \mu)(\epsilon_{xx} + \epsilon_{yy} + \epsilon_{zz})^2 \quad (2)$$

$$E_S = \mu(\nabla \times \mathbf{u}(t))^2 = \mu(2\omega_x^2 + 2\omega_y^2 + 2\omega_z^2), \quad (3)$$

where (x, y, z) are a set of orthogonal reference axes. Once E_P and E_S have been obtained, it is then possible to analyze the energy partition as the ratio of the two. Because of the strong fluctuations, the energy was smoothed, before computing the ratio, using a moving window.

In this section, we show the evolution of the energy partition ratio observed at a distance of 2 km from the source, in two cases (Fig. 5).

In both case study, Fig. 5 (a) and (b), we solved the RTE and compared the results with the SEM computations. The main difference between the two simulations, is that while in the SEM simulations the source function is a Ricker wavelet, in the Monte Carlo simulations the source is a single pulse. To align with this difference, an additional simulation was conducted using a completely homogeneous medium. The solution of the radiative transfer equation was subsequently convolved with the observed source function at a 5 km distance to simulate the same source conditions of the SEM simulations (Celorio et al., 2022). This allowed us to analyze the entire evolution of the partition ratio, starting from the ballistic arrivals. In both cases we observe an excellent match between the results obtained from SEM simulations and the energy ratio predicted by RTE. In the first case, where $\epsilon = 10\%$, we observe the dynamic of energy partition up to a certain time lapse, which is insufficient to achieve complete equilibrium, while in the second case, where $\epsilon = 25\%$, we can observe the transition up to almost the asymptotic

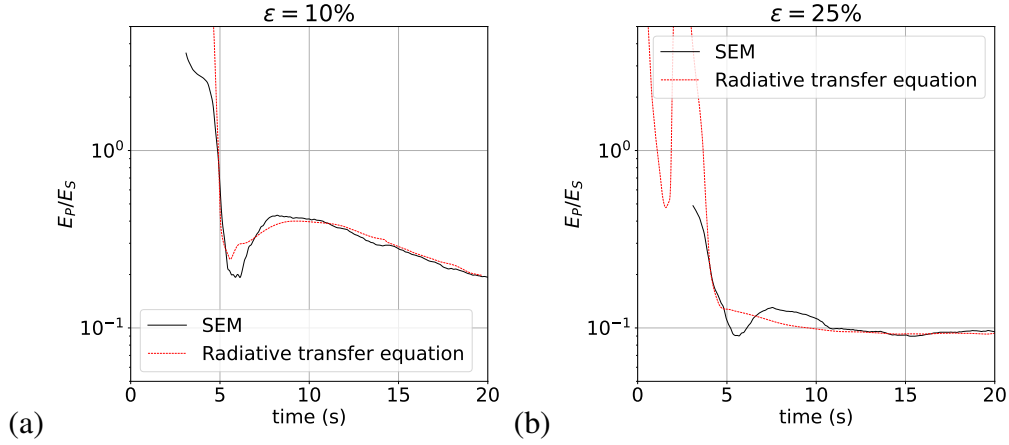


Figure 5: Energy partition comparison, SEM computation and radiative transfer equation solved with the Born approximation. (a) $\epsilon = 10\%$ (b) $\epsilon = 25\%$. The ratio observed at 50 locations is plotted in light gray to illustrate the fluctuations around the mean.

limit, $v_s^3/(2v_p^3) \sim 0.1$.

A note here concerns the solution of the radiative transfer equation (RTE) in the 25% case. Theoretically the Born approximation is expected to be valid in the regime $(ka\epsilon)^2 \ll 1$ with k the wavenumber and a the correlation length of fluctuations (Rytov et al., 1989). In the case $\epsilon = 0.25$, we certainly reach the theoretical limit of applicability ($k^2 a^2 \epsilon^2 \approx 0.6$). In practice, the application threshold appears to be flexible. In this study, we demonstrate that the Born approximation appears to be valid up to 25% velocity perturbations as far as energy partition ratios are concerned.

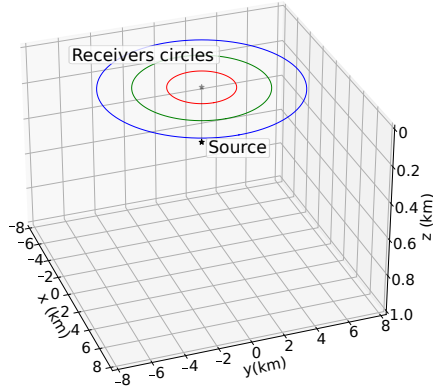


Figure 6: Source-receiver configuration. 1500 receivers have been deployed on each circle, centered at the source location.

3 Simulation in a Half-Space Medium

In this section, we investigate the energy evolution of the three observables in the two case studies, $\epsilon = 10\%$ and $\epsilon = 25\%$, under the assumption of an isotropic source incorporating the presence of a free surface. The source-receivers configuration shown in Fig. 6 (a) was used. 1500 receivers were arranged along concentric circles starting from a radius of 2 km, increasing by 1 km. The source was positioned at the center of these circles but at a depth of 300 m.

The parameters used in these simulations are once again those listed in the Supplementary Material, Table S1.

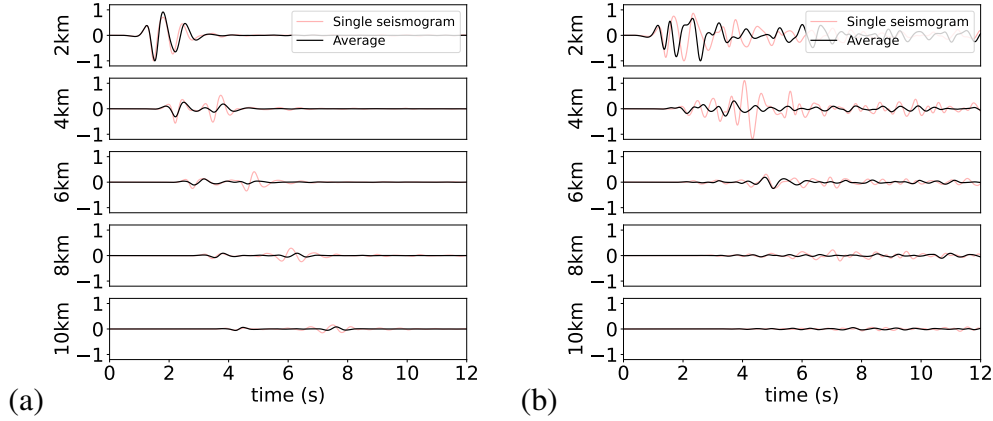


Figure 7: Comparison of two simulations in a heterogeneous half-space medium with $\epsilon = 10\%$ (a) and $\epsilon = 25\%$ (b). Radial field observed increasing source-to-receiver distance. In the first case (a), P and Rayleigh waves are clearly visible, while in the second case (b), the average is not efficient enough to remove the fluctuations, and therefore the presence of coherent body and surface waves does not appear clearly. The signals have been filtered between 0.9 and 2.8Hz.

3.1 Mean free path

The mean field was calculated as before, by averaging the radial component at a defined distance from the source. Fig. 7 presents the mean field obtained from the two simulations with $\epsilon = 10\%$ (a) and $\epsilon = 25\%$ (b).

In the first case, the main components of the wavefield are clearly visible; ballistic arrivals, i.e. P waves, and, from 5 km onwards, Rayleigh waves can be distinctly observed. In the second case, however, strong fluctuations obscure these components, resulting in a less distinct average compared to the full-space simulation, as shown in Fig. 3(a). This occurs because, in the full-space medium, the receivers were arranged on a spherical surface and were more widely spaced. In

contrast, the reduced distance between receivers in this case results in nearby receivers capturing very similar signals, making it difficult for the averaging process to fully eliminate the fluctuations.

In this case, the mean free path was calculated for both P waves and Rayleigh waves, with a comparison to previous results from the full-space medium for P waves. The results show that the mean free path for P waves in the half-space (P_{HS}), up to approximately 2.4 Hz, is nearly parallel to that observed in the full-space medium, with a value about 0.5 times as large as the full-space mean free path (P_{FS}). This difference is due to the additional conversion from P waves to Rayleigh waves in the half-space. Following the same reasoning as in Margerin et al. (2019); Xu et al. (2022), we may estimate that in the frequency range investigated in our study, the scattering conversion from P to Rayleigh waves in the close vicinity of the free surface is about as efficient as the sum of the P-to-P and P-to-S scattering conversions. Rayleigh waves (RW), on the other hand, appear to have a mean free path that falls between the one of P_{HS} and P_{FS} .

3.2 Transition from multiple scattering to diffusion

The decay of energy, calculated as described in paragraph 2.2, shows that while the dynamics of the observables differ from the full space medium case due to the influence of surface waves, the transition to the diffusive regime occurs later. Specifically, for the simulation with $\epsilon = 10\%$, this transition occurs at a lapse time of about 18 seconds (Fig. 9(a)), and for $\epsilon = 25\%$, at a lapse time of about 10 seconds (Fig. 9(b)). In the latter case, the decay follows a $t^{-3/2}$ trend, consistent

with the predictions of Margerin et al. (2019). For comparison, we also present decay rates proportional to t^{-1} and t^{-2} . These results suggest the dominance of body waves in the transport of energy in the coda at long lapse-time.

3.3 Energy partition ratio

In this section, we compared the energy partition ratio E_s/E_p observed in the SEM simulations of the two case study with the one predicted by Hennino in the framework of equipartition theory (Hennino et al., 2001). We remind the reader that equipartition is a fundamental principle in multiple-scattering which stipulates that, at sufficiently long lapse time, the wave energy becomes equally distributed among all the propagation modes of the medium. We refer to Weaver (1990); Ryzhik et al. (1996); de Hoop et al. (2022) for theoretical arguments and to Khazaie et al. (2017) for a detailed numerical study in 3-D based on SEM simulations.

In the first case, Fig. 10 (a), where $\epsilon = 10\%$, we observe the arrival of P waves at about 2.5 seconds, the arrival of the S and Rayleigh wave train at about 5 seconds, and then we see the ratio rise to about 0.3 before starting to decrease. In this case, the asymptotic limit is not fully reached at the end of the simulation but the temporal evolution of the energy ratio suggests slow convergence towards the expected limit.

By contrast, in Fig. 10 (b), after the arrival of the S and Rayleigh waves, the ratio stabilizes around the expected value, approximately 0.14 for the medium analyzed (Hennino et al., 2001). For further examples and detailed discussions,

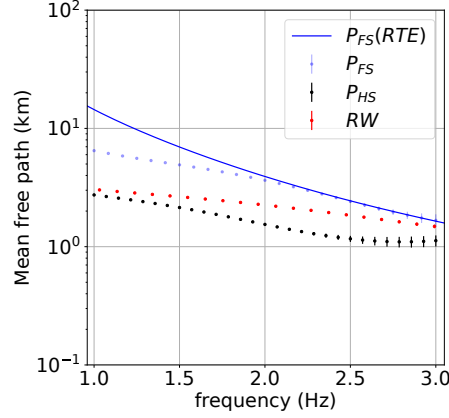


Figure 8: Mean free paths of the half-space, for P (P_{HS}) and Rayleigh waves (RW). Comparison with P mean free path observed in the full space using SEM (P_{FS}) and RTE ($P_{FS}(RTE)$).

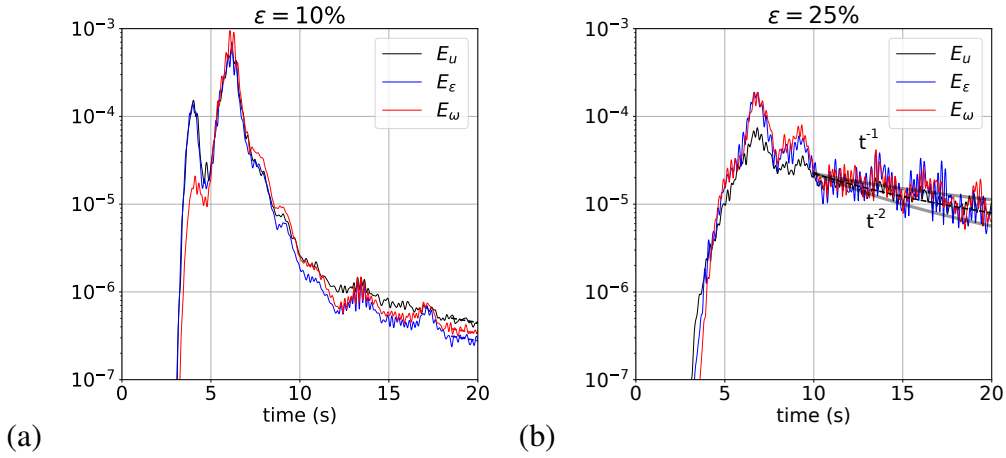


Figure 9: Decay rate of the late coda in a half-space medium. Comparisons of the displacement energy $E_u = u_x^2 + u_y^2 + u_z^2$, rotation energy $E_\omega = \omega_x^2 + \omega_y^2 + \omega_z^2$, and strain energy $E_\epsilon = \epsilon_{xx}^2 + \epsilon_{yy}^2 + \epsilon_{zz}^2$ in the two cases. Envelopes have been computed for a source-to-receiver distance of 2 km. The transition to the diffusive regime starts at about 18 seconds in the $\epsilon = 10\%$ simulation (a) and at about 10 seconds in the $\epsilon = 25\%$ simulation (b). In this case, we show the decay rate, proportional to $t^{-3/2}$, which is consistent with predictions of Margerin et al. (2019). For comparison purposes, we also show the decay proportional to t^{-1} and t^{-2} .

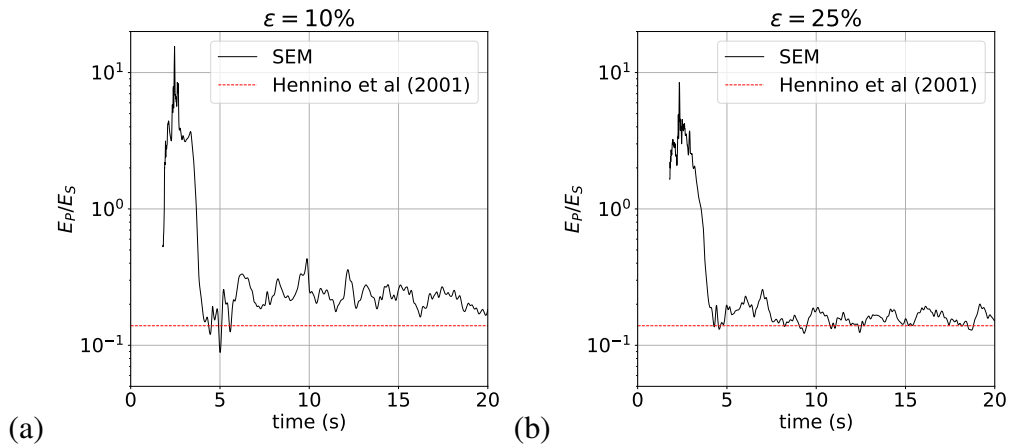


Figure 10: Energy partition ratio of the two case with $\epsilon = 10\%$ (a) and $\epsilon = 25\%$ (b) at the free surface. The asymptotic limit was obtained by [Hennino et al. \(2001\)](#).

the reader may consult [Khazaie et al. \(2017\)](#).

4 Energy envelope analysis

In this section, we present an analysis of the evolution of energy of the radial and transverse components of three observables: displacement $u(t)$, linear strain $\epsilon(t)$, and rotation $\omega(t)$. We examine two case studies: first, the full-space medium, and second, the half-space medium. By contrast with previous numerical works focusing on the capability of RTE to correctly model a broad variety of scattering media (e.g. [Przybilla et al., 2006](#); [Celorio et al., 2022](#)) our interest is on the potential of wavefield gradients as new observables to characterize the scattering mechanisms in heterogeneous media. For an application to seismic data, the reader is referred to [Gaebler et al. \(2015\)](#) who employ Monte-Carlo solutions of RTE to model rotational motions in the teleseismic P-coda detected by a ringlaser.

4.1 Full space medium

The energy of individual components of the observables was averaged at specific distances from the source. In this section we analyze separately the two cases with increasing strength of heterogeneity $\epsilon = 10\%$ and 25% , the case with $\epsilon = 17\%$ is shown in the Supplementary Material, Fig. S4.

In the case of least scattering, as shown in Fig. 11, a strong ballistic arrival is visible in the radial component, followed by a train of S-waves visible in the other components. Even though the source is characterized by an isotropic moment tensor, heterogeneities near the source can generate conversion from P-wave to S-wave. If these waves are generated close to the source, they appear to propagate as if they were emitted directly from the source itself. The observation of S-waves arrival in a heterogeneous medium, given an isotropic source, is consistent with the works of Hirakawa et al. (2016); Margerin (2017) and appears in all the cases analyzed. To confirm this hypothesis, it is possible to notice that this contribution is absent in the divergence of the field, Fig. 11 (b).

As the scattering increases, the transition to multiple scattering occurs more rapidly. In Fig. 12, we observe that the ballistic arrivals are less pronounced and the contribution of S waves is spread over longer time windows. At a distance of 8 km, for instance, a perfect example of a diffusive regime is shown. In this case, the direct waves are absent and the envelope begins with a smooth increase of the energy, characteristic of the diffusive regime.

This progression is closely linked to the phenomenon of mode conversions and depolarization. The latter refers to the alteration of the original polarization direc-

tion of seismic waves as they propagate through a medium. Depolarization arises from interactions between seismic waves and heterogeneities in the medium. In a complex medium with numerous heterogeneities, repeated interactions lead to a cumulative loss of information about the source's initial polarization, ultimately resulting in complete depolarization. The analysis of the different observables has revealed substantial differences when comparing displacement-strain with rotations. In the first two observables, displacement and strain, as shown in Fig. 11 (a) and (b), depolarization occurs a few seconds after the arrival of S waves. For instance, at a distance of 5 km, depolarization happens approximately 2 seconds after the arrival of S waves. While the observation is the same for strain, Fig. 11 (b), a significant difference is noted in the case of rotations, Fig. 11 (c). In this case, considering the same distance, as shown in Fig. 11 (b), depolarization occurs about 8 seconds after the arrival of the S waves. Given that wavefield rotations are sensitive solely to S waves, this analysis allows us to show that an isotropic source, which generates only P waves, produces a conversion to S waves, essentially along the transverse axes rather than along the axis directed toward the source itself, hence mimicking a sort of "ghost" S source. However, with increasing scattering, as shown in Fig. 12 (c), the depolarization time of the rotations decreases.

4.2 Half-space medium

In this case, the presence of the free surface significantly alters the dynamics of the evolution of signal energy due to the presence of Rayleigh surface waves. In

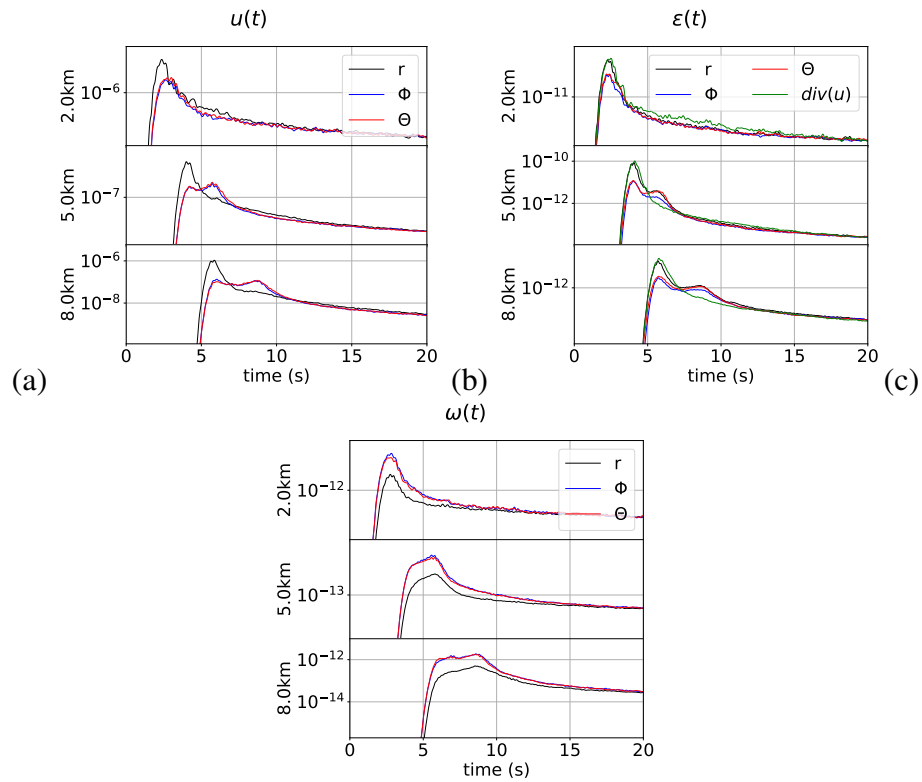


Figure 11: Envelope simulation based on SEM with $\epsilon = 10\%$ in full space medium. Comparison of the energy evolution of the radial and transverse components of the displacement (a), linear strain (b) and rotation (c).

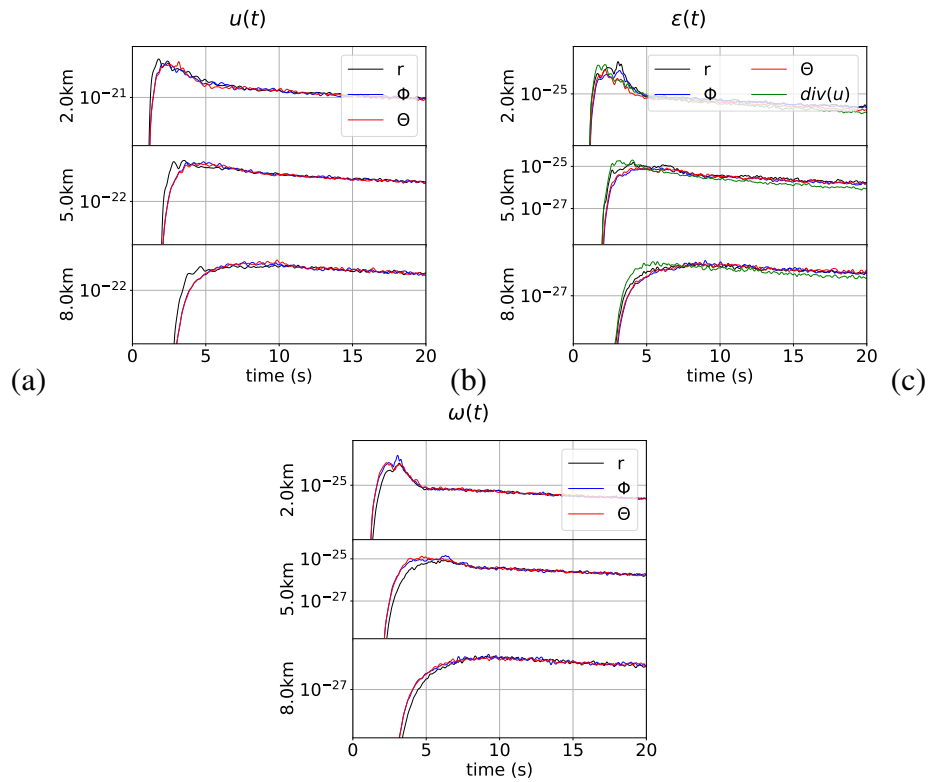


Figure 12: Envelope simulations based on SEM with $\epsilon = 25\%$ in full space medium. Comparison of the energy evolution of the radial and transverse components of the displacement (a), linear strain (b) and rotation (c).

this configuration, the receivers have been rotated towards the source's epicenter, and not the source location. This means that considering the widely used RTZ coordinate system, z corresponds to Z , Φ corresponds to T , and r to R .

In Fig. [13](#), we show the evolution of the three radial and transverse components of displacement (a), strain (b), and rotation (c) in the simulation where $\epsilon = 10\%$.

In the displacement, we observe the presence of P-waves polarized along the radial direction, followed by the arrival of S-waves and Rayleigh waves. The presence of Rayleigh waves becomes clearly visible, especially at distances greater than 5 km from the source. At these distances, it can be seen that the z and Φ components have a lower amplitude than r . Specifically, r , which corresponds to the radial axis, is energized by P and Rayleigh waves, polarized in the vertical-radial plane.

In the strain (b), two peaks related to body waves and Rayleigh waves are still observed. However, an offset can be observed between the strain energy of the vertical component and the other components. This difference is due to free surface conditions. Specifically, at free surface, the three components of the stress, along the three axes $i = x, y, z$, the stress component τ_{iz} must be zero. For the vertical component we can write ([Aki and Richards, 2002](#)):

$$\tau_{zz} = \lambda \left(\frac{\partial u_x}{\partial x} + \frac{\partial u_y}{\partial y} + \frac{\partial u_z}{\partial z} \right) + 2\mu \frac{\partial u_z}{\partial z} = \lambda \nabla \cdot u + 2\mu \frac{\partial u_z}{\partial z} = 0 \quad (4)$$

This means that:

$$\nabla \cdot u = -\frac{2\mu}{\lambda} \frac{\partial u_z}{\partial z} \quad (5)$$

For a Poisson medium, $2\mu/\lambda = 2$. Which means that the amplitude of the vertical strain component is approximately half that of the signal's divergence, and four times less when considering the energy. In the simulations, we find full agreement with the theory. Apart from this effect, the energy dynamics of the strain are similar to those observed in the displacement.

In the rotations (c), we observe a large peak on the Φ component, due to the arrival of Rayleigh waves, as expected, and a similar dynamic to that observed in the full space medium case Fig. [11](#) and Fig. [12](#). The difference here is that the vertical component z shows much less energy compared to the other two components. This is due to the fact that SH waves are not produced by the source but only through conversion.

In the case of $\epsilon = 25\%$, we observe a dynamics similar to that shown in the previous case across all observables, with the difference that, due to the lower conversion times, depolarization is accelerated. In the displacement, Fig. [14](#) (a), we see very quick depolarization. At 2 and 8 km, a small increase in energy is noticeable in the vertical component z , attributable to Rayleigh waves. This behavior is not present in strain (b), because of the free surface conditions, also in this case the vertical component is the less energetic one. In the rotations, it is observed that the Φ component, like in the previous case, peaks with the arrival of Rayleigh waves and then depolarizes. At distances greater than 5 km, it is also

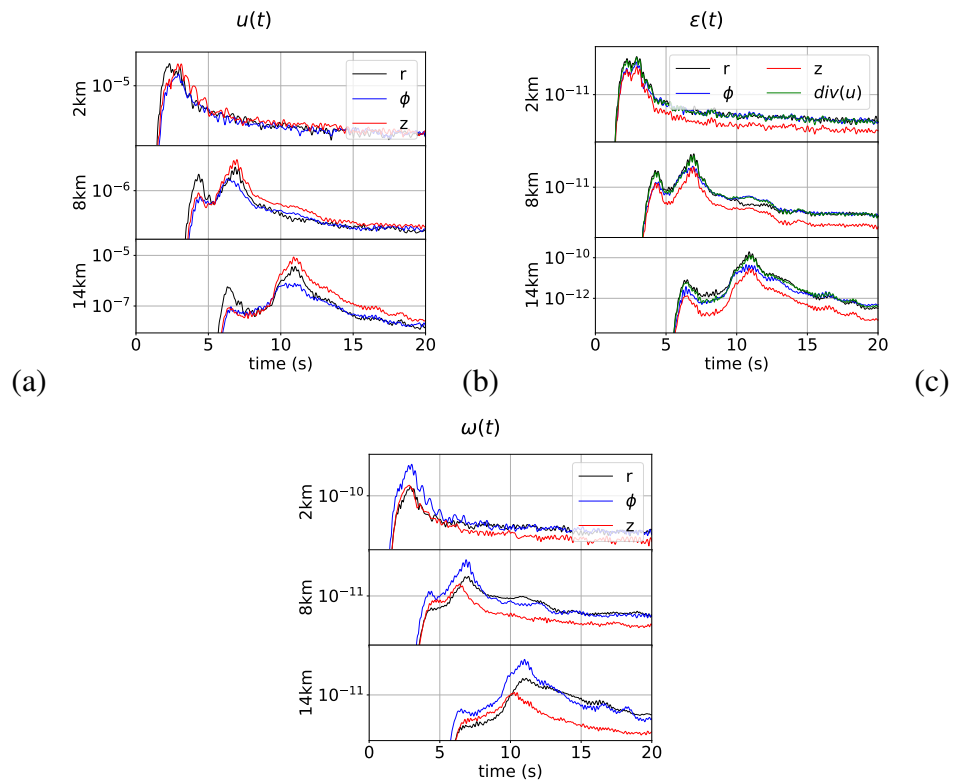


Figure 13: Envelope simulations based on SEM with $\epsilon = 10\%$ in a half space medium and isotropic source. Comparison of the energy evolution of the radial and transverse components of the displacement (a), linear strain (b) and rotation (c).

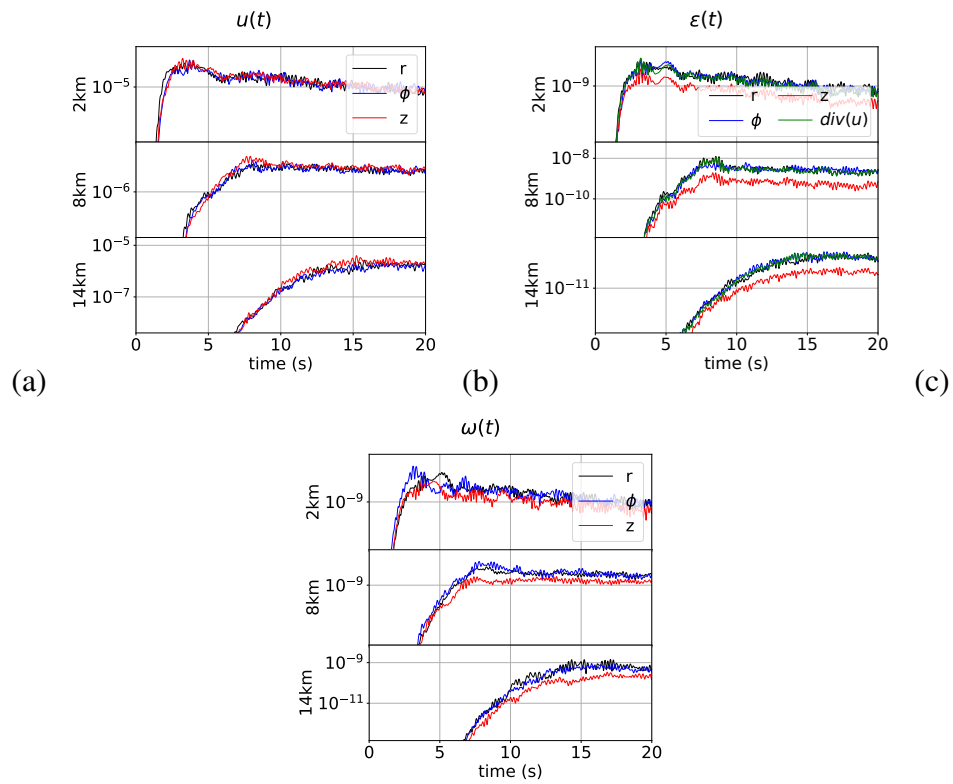


Figure 14: Envelope simulations based on SEM with $\epsilon = 25\%$ in a half space medium and isotropic source. Comparison of the energy evolution of the radial and transverse components of the displacement (a), linear strain (b) and rotation (c).

observed that the z component takes much longer time to increase in energy and overlap with the other two components, to reach depolarization.

The dynamic of the strain is, as in the previous case, similar to the one of the displacement, with the difference of the lower amplitude of the vertical component of the strain due to the free surface conditions [14](#)(b).

The analysis of another case, with $M_{zz} \neq 0$ is provided in the Supplementary Material, Fig. S5.

5 Conclusions

This study investigates the propagation of seismic waves in a 3D uniform heterogeneous medium through numerical simulations of the Wave Equation and the Radiative Transfer Equation (RTE).

The work is divided into two main parts. The first part of this study focuses on the reliability assessment of two simulation methods. While earlier studies ([Frankel and Clayton, 1986](#); [Przybilla et al., 2006](#); [Imperator and Mai, 2012](#); [Obermann et al., 2013, 2016](#); [Emoto and Sato, 2018](#); [Celorio et al., 2022](#), etc...) have mostly addressed individual aspects of wave propagation in heterogeneous media, this work offers a novel contribution by providing a systematic comparison between the two approaches in 3D full elasticity with respect to fundamental parameters of the multiple scattering such as mean free paths or P-to-S energy partition. Heterogeneity fluctuations ranging from 10 to 25 percent are considered in two scenarios: a full-space medium (Section [2](#)) and a half-space medium

(Section 3). The comparison between the methods is conducted in terms of the values of the scattering mean free path, the transition from multiple scattering to the diffusive regime (via energy decay analysis), and the P-S energy partition ratio. The results show excellent agreement between the two methods in the range of frequency between 0.9 and 2.8Hz. The high accuracy demonstrated by SEM simulations opens new opportunities for their application in inversion studies.

In Full Waveform Inversion (FWI), accurate forward modeling of wave scattering enhances the reliability of the resulting inverted models and expands their applicability to regimes dominated by multiple scattering and diffusion. Furthermore, energy-envelope inversions of field data could be performed using SEM simulations, enabling the estimation of the medium scattering parameters.

The second part of this study analyzes the same two cases of scattering strength (Paragraph 4), investigating the energy evolution of the three components of displacement, strain, and rotation produced by an isotropic moment tensor source. The analysis reveals in both cases, that, even though the source does not directly generate S waves, a 'ghost' S source is produced through wave conversion, as previously observed by [Hirakawa et al. \(2016\)](#). This 'ghost' source results from the conversion of P waves to S waves near the source, generating S waves that induce rotations along the transverse axis. However, rotations appear to be very weakly generated along the radial or propagation direction, suggesting that even in an isotropic, uniformly heterogeneous medium, the conversion times among the three directions may differ over finite lapse times. In conclusion, it is observed that displacement and strain components lose their polarization shortly after the

arrival of S-waves, while the rotation components retain the source-induced polarization for significantly longer times, persisting for up to twice the Thouless time in the 10% perturbation scenario, where this can be observed. This behavior may be attributed to the fact that displacement and strain contain contributions from both P and S wavefields, unlike rotations, which are sensitive only to S waves. The combined contributions of both fields in displacement and strain can, in fact, obscure the behavior of the S wavefield. This implies that rotation measurements can provide valuable information about the source and the direction of propagation of the waves. A characteristic that can be exploited to impose an additional constraint on the source mechanism, the waves propagation direction and their polarization.

Acknowledgments

This work is supported by the European Union's Horizon 2020 research and innovation program under the Marie Skłodowska-Curie grant agreement No 955515 and by The European Research Council under the European Union Horizon 2020 research and innovation program (Grant agreements no 742335, F-IMAGE for M.B. and M.C.).

Author contribution statement

Conceptualization: MC, MB. Data curation: MB. Formal analysis: MB, MC. Funding acquisition: MC. Investigation: MB, MC. Methodology: MB, MC, RB. Project administration: MC. Resources: RB. Software: RB. Supervision: MC. Validation: MC, RB. Visualization: MB. Writing – original draft: MB. Writing – review & editing: MC, RB.

Data Availability Statement

Seismograms generated by wave equation simulations, along with the results of the radiative transfer equation for the full-space media, are available at:

<https://zenodo.org/records/15229635>. Seismograms corresponding to the half-space media are available at: <https://zenodo.org/records/15240713>.

References

- Aki, K. and Richards, P. G. (2002). *Quantitative Seismology: Theory and Methods*. University Science Books, Sausalito, CA, 2nd edition.
- Celorio, M., Chaljub, E., Margerin, L., and Stehly, L. (2022). Propagation of 2-d sh waves in random media: Insights from ab initio numerical simulations and transport theory. *Frontiers in Earth Science*, 10.
- de Hoop, M. V., Garnier, J., and Sølna, K. (2022). System of radiative trans-

- fer equations for coupled surface and body waves. *Zeitschrift für angewandte Mathematik und Physik*, 73(5):177.
- Emoto, K. and Sato, H. (2018). Statistical characteristics of scattered waves in three-dimensional random media: comparison of the finite difference simulation and statistical methods. *Geophysical Journal International*, 215(1):585–599.
- Frankel, A. and Clayton, R. W. (1986). Finite difference simulations of seismic scattering: Implications for the propagation of short-period seismic waves in the crust and models of crustal heterogeneity. *Journal of Geophysical Research: Solid Earth*, 91(B6):6465–6489.
- Gaebler, P. J., Sens-Schönfelder, C., and Korn, M. (2015). The influence of crustal scattering on translational and rotational motions in regional and teleseismic coda waves. *Geophysical Journal International*, 201(1):355–371.
- Hennino, R., Trégourès, N., Shapiro, N. M., Margerin, L., Campillo, M., van Tiggelen, B. A., and Weaver, R. L. (2001). Observation of equipartition of seismic waves. *Phys. Rev. Lett.*, 86:3447–3450.
- Hirakawa, E., Pitarka, A., and Mellors, R. (2016). Generation of shear motion from an isotropic explosion source by scattering in heterogeneous media. *Bulletin of the Seismological Society of America*, 106(5):2313–2319.
- Igel, H. (2017). *Computational Seismology: A Practical Introduction*. Oxford University Press, Oxford, UK.

- Imperator, W. and Mai, P. M. (2012). Broad-band near-field ground motion simulations in 3-dimensional scattering media. *Geophysical Journal International*, 192(2):725–744.
- Khazaie, S., Cottureau, R., and Clouteau, D. (2017). Numerical observation of the equipartition regime in a 3d random elastic medium, and discussion of the limiting parameters. *Computers & Geosciences*, 102:56–67.
- Komatitsch, D. and Tromp, J. (1999). Introduction to the spectral element method for three-dimensional seismic wave propagation. *Geophysical Journal International*, 139(3):806–822.
- Komatitsch, D. and Vilotte, J.-P. (1998). The spectral element method: An efficient tool to simulate the seismic response of 2d and 3d geological structures. *Bulletin of the Seismological Society of America*, 88(2):368–392.
- Maeda, T., Sato, H., and Nishimura, T. (2008). Synthesis of coda wave envelopes in randomly inhomogeneous elastic media in a half-space: single scattering model including rayleigh waves. *Geophysical Journal International*, 172(1):130–154.
- Margerin, L. (2005). *Introduction to Radiative Transfer of Seismic Waves*, pages 229–252. American Geophysical Union (AGU).
- Margerin, L. (2017). Computation of green’s function of 3-d radiative transport equations for non-isotropic scattering of p and unpolarized s waves. *Pure and Applied Geophysics*, 174(11):4057–4075.

- Margerin, L., Bajasas, A., and Campillo, M. (2019). A scalar radiative transfer model including the coupling between surface and body waves. *Geophysical Journal International*, 219(2):1092–1108.
- Nakahara, H. and Yoshimoto, K. (2011). Radiative transfer of elastic waves in two-dimensional isotropic scattering media: Semi-analytical approach for isotropic source radiation. *Earth, Planets and Space*, 63(6):459–468.
- Obermann, A., Planès, T., Hadziioannou, C., and Campillo, M. (2016). Lapse-time-dependent coda-wave depth sensitivity to local velocity perturbations in 3-d heterogeneous elastic media. *Geophysical Journal International*, 207(1):59–66.
- Obermann, A., Planès, T., Larose, E., Sens-Schönfelder, C., and Campillo, M. (2013). Depth sensitivity of seismic coda waves to velocity perturbations in an elastic heterogeneous medium. *Geophysical Journal International*, 194(1):372–382.
- Pham, N. D., Igel, H., Wassermann, J., Käser, M., de la Puente, J., and Schreiber, U. (2009). Observations and modeling of rotational signals in the p coda: Constraints on crustal scattering. *Bulletin of the Seismological Society of America*, 99(2B):1315–1332.
- Przybilla, J., Korn, M., and Wegler, U. (2006). Radiative transfer of elastic waves versus finite difference simulations in two-dimensional random media. *Journal of Geophysical Research: Solid Earth*, 111(B4).

- Rodgers, A. J., Petersson, N. A., and Sjogreen, B. (2010). Simulation of topographic effects on seismic waves from shallow explosions near the north korean nuclear test site with emphasis on shear wave generation. *Journal of Geophysical Research: Solid Earth*, 115(B11).
- Rytov, S. M., Kravtsov, Y. A., and Tatarskii, V. (1989). *Principles of statistical radiophysics: wave propagation through random media*. Springer.
- Ryzhik, L., Papanicolaou, G., and Keller, J. B. (1996). Transport equations for elastic and other waves in random media. *Wave Motion*, 24(4):327–370.
- Sato, H. and Fehler, M. C. (2012). *Seismic Wave Propagation and Scattering in the Heterogeneous Earth: Second Edition*. Springer, Heidelberg, 2nd edition.
- Shapiro, B. (1999). New type of intensity correlation in random media. *Phys. Rev. Lett.*, 83:4733–4735.
- Sánchez-Sesma, F. J. and Campillo, M. (1991). Diffraction of p, sv, and rayleigh waves by topographic features: A boundary integral formulation. *Bulletin of the Seismological Society of America*, 81(6):2234–2253.
- Tregoures, N. P. and van Tiggelen, B. A. (2002). Quasi-two-dimensional transfer of elastic waves. *Physical Review E*, 66(3):036601.
- Trinh, P.-T., Brossier, R., Métivier, L., Tavard, L., and Virieux, J. (2019). Efficient time-domain 3d elastic and viscoelastic full-waveform inversion using a spectral-element method on flexible cartesian-based mesh. *Geophysics*, 84(1):R75–R89.

- Turner, J. A. and Weaver, R. L. (1994). Radiative transfer and multiple scattering of diffuse ultrasound in polycrystalline media. *The Journal of the Acoustical Society of America*, 96(6):3675–3683.
- Virieux, J. and Operto, S. (2009). An overview of full-waveform inversion in exploration geophysics. *GEOPHYSICS*, 74(6):WCC1–WCC26.
- Weaver, R. (1990). Diffusivity of ultrasound in polycrystals. *Journal of the Mechanics and Physics of Solids*, 38(1):55–86.
- Xu, Z., Margerin, L., and Mikesell, T. D. (2022). Monte carlo simulations of coupled body-and rayleigh-wave multiple scattering in elastic media. *Geophysical Journal International*, 228(2):1213–1236.
- Zeng, Y. (2006). Scattered surface wave energy in the seismic coda. *Pure and applied geophysics*, 163:533–548.

Simulation of multiply scattered elastic waves with 3D wave-equation and radiative transfer equation for displacements and their gradients.”

Mirko Bracale¹, Romain Brossier¹, Ludovic Margerin², Michel Campillo¹

¹ISTerre, Université Grenoble Alpes, CNRS, Université Savoie Mont Blanc, IRD, Université Gustave Eiffel, Grenoble, France

²Institut de recherche en astrophysique et planétologie, IRAP/OMP - CNRS, CNES, Université Toulouse III - Paul Sabatier,

Toulouse, France

Contents of this file

1. Text S1 to S5
2. Figures S1 to S5
3. Table S1

Text S1. Numerical Methods for Simulating Seismic Waves in Heterogeneous Media

In this section, we provide an overview of the theory behind the simulations used in this study to model the propagation and scattering of seismic waves in a heterogeneous medium. This section aims to present key concepts that are essential for understanding these simulations. Detailed information on these methods can be found in the cited literature.

Solving the Wave equation:

Numerical simulations of the wave equation are used to compute the ground motion generated by the propagation of waves through a medium with defined elastic properties. These simulations are widely employed in seismology to either model ground motion or invert real data to compute the medium properties using Full Waveform Inversion virieux2009. The partial differential equation of the wave equation is solved numerically in a discretized space and time, giving the ground motion (i.e., synthetic seismograms) at specifically defined positions.

Several methods exist to solve the wave equation, the main ones being the finite difference method alterman1968, the finite element bruce1972 and its well-known version "spectral element method" Komatitsch1997, or the pseudo-spectral method Fornberg (1987). For a detailed review of these methods, refer to Igel (2017).

In this study, we solved the elastic wave equation using the Spectral Element Method (SEM), introduced in seismology by Komatitsch (1997). The implementation used in this work, the SEM46 code, is based on the subsequent works komatitsch1998, Komatitsch1999, which use a particular formulation on Cartesian-based deformed mesh trinh2019.

The spectral element method offers a very good compromise between the computational cost and the accuracy of the solution compared to standard finite element methods, in particular in the presence of free-surface boundary condition trinh2019

The elastic wave equation is given by Aki2002:

$$(I) \quad \rho \frac{\partial^2 u_i(x, t)}{\partial t^2} = \frac{\partial \sigma_{ij}(x, t)}{\partial x_j} + f_i(x, t), \quad (1)$$

$$(II) \quad \sigma_{ij}(x, t) = c_{ijkl} \epsilon_{kl}(x, t) + \tau_{ij}(x, t),$$

where ρ is the density, σ_{ij} is the Cauchy stress tensor, f_i is the source term, c_{ijkl} is the stiffness tensor, ϵ_{kl} is the infinitesimal strain, and τ_{ij} is the stress glut.

The weak form of this wave equation is considered, employing Lagrange polynomials as basis functions to represent the wavefield in hexahedron-based meshes, and Gauss-Lobatto-Legendre (GLL) quadrature for the numerical integration. This equation can then be rewritten in the semi-discrete case as follows Komatitsch1997:

$$\mathbf{M} \frac{\partial^2 \mathbf{u}}{\partial t^2} = -\mathbf{K} \mathbf{u} + \mathbf{F}, \quad (2)$$

where \mathbf{M} is the mass matrix, \mathbf{K} is the stiffness matrix, and \mathbf{F} is the source term.

A key advantage of this formulation is that the mass matrix \mathbf{M} is diagonal by construction. In addition, highly efficient algorithms allow to compute the product between \mathbf{K} and \mathbf{u} in a matrix-free fashion deville2002.

The definition of a seismic source is specified in terms of source time function and mechanical mechanism.

A crucial aspect of building an heterogeneous medium to solve the wave equation is the need to define the elastic properties of the medium, typically expressed in terms of seismic wave propagation velocities and density at each point of the space. This is done at each GLL point in our implementation. Following this method, the correlation between these parameters is unconstrained, allowing the definition of a medium in which the elastic parameters vary independently at each point in space, thereby defining a medium characterized by different scattering properties thorough. This aspect represents a fundamental difference with respect to how the medium must be defined for solving the Radiative Transfer Equation.

Solving the Radiative Transfer Equation:

The radiative transfer equation describes the attenuation of specific intensity of seismic waves, due to their propagation in a heterogeneous medium. In seismology, in the scalar case, this equation assumes the following form weaver1990,ryzhik1996,turner1994,margerin2005 :

$$\frac{1}{v} \frac{dI(t, \mathbf{r}, \hat{s})}{dt} = -\frac{I(t, \mathbf{r}, \hat{s})}{l} + G(t, \mathbf{r}, l, \hat{s}) + S(t, \mathbf{r}, \hat{s}) \quad (3)$$

The first term on the right, represents the attenuation of the intensity $I(t, \mathbf{r}, \hat{s})$ of a beam of waves propagating in the direction \hat{s} due to scattering, given the mean free path l . The term $\mathbf{G}(t, \mathbf{r}, \hat{s}, \hat{s}')$ accounts for the gain of energy that neighboring beams of waves propagating in direction \hat{s}' deflect toward the direction \hat{s} , and $S(t, \mathbf{r}, \hat{s})$ is the source term. Full expression of the vector form for elastic waves can be found in Tregoures and van Tiggelen (2002); Margerin et al. (2019); Margerin (2005).

Extensively, in the scalar case, the gain term $\mathbf{G}(t, \mathbf{r}, \hat{s}, \hat{s}')$ can be written as:

$$G(t, \mathbf{r}, l, \hat{s}) = \frac{v dt}{l} \int p(\hat{s}, \hat{s}') I(t, \mathbf{r}, \hat{s}') d^2 \hat{s}' \quad (4)$$

The term $p(\hat{s}, \hat{s}')$ defines the probability of a ray propagating in the direction \hat{s}' being deflected in the direction \hat{s} . This probability depends on the distribution and size of the heterogeneities and is derived from the autocorrelation function (ACF), which governs the spatial correlation of the elastic parameters. In the simulation used in this study this term is computed using the Born Approximation [abubakirov1990,hoshiba1991](#), which involves approximating the scattering function to the second order. This is a fundamental aspect of radiative transfer theory. It requires the propagating medium to have uniform scattering properties throughout the entire medium and, consequently, spatially correlated heterogeneities. Such a medium is generally referred to as a "heterogeneous uniform medium." The code used to solve the RTW was developed by Margerin, with details provided in Margerin et al. (2000).

Observations on scattering and comparison between Elastic Wave and Radiative Transfer Equation Simulations:

Simulating seismic waves in a heterogeneous medium presents significant challenges due to the complex interactions between waves and the medium's heterogeneities. As waves propagate, they transition through distinct "scattering regimes," depending on the extent and nature of these interactions [SatoFehler2012](#).

In the single scattering regime, waves typically interact with heterogeneities only once before reaching the receiver, resulting in relatively simple wave paths. Conversely, in the multiple scattering regime, waves interact with several heterogeneities, leading to more complex paths and significant alterations in wave properties. This regime is a key contributor to the generation of the seismic coda [aki1975](#). As the number of interactions increases further, waves enter the diffusion regime, where their behavior can be described by the diffusion equation [SatoFehler2012](#). In this regime, the energy flow becomes smooth and evenly distributed, contrasting with the

peaked distributions observed in ballistic arrivals. Notably, ballistic arrivals remain visible in the single and multiple scattering regimes, although they are partially affected by scattering.

The transition between these regimes is primarily governed by the wavenumber of the propagating waves, k , the distance from the source, r , the mean free path, l , the size of the heterogeneities a , and the strength, ϵ , of the perturbations SatoFehler2012. In order to solve the RTE, the last two parameters must remain constant throughout the entire medium, or alternatively, the medium can be divided into different regions with smooth transitions between them. However, it is crucial that the correlation of heterogeneity follows a specific autocorrelation function, which is necessary to compute the scattering cross section.

To enable a meaningful comparison between RTE and Elastic Wave solutions, it is necessary to consider a medium whose elastic and scattering properties are the same. For this reason, although SEM simulations do not inherently require a correlation between medium heterogeneities, a medium with correlated heterogeneities was also employed in SEM simulations. To construct such a medium, heterogeneities characterized by a Gaussian white noise distribution of propagation velocity were initially considered. This medium was then filtered through spatial convolution with a Von Kármán function, with a fixed correlation length.

Following this procedure, the medium was analyzed to verify its scattering statistical properties. This step is essential to ensure that the applied procedure generated the desired medium. Specifically, both the autocorrelation of the velocity model and its power spectral density spectrum were evaluated. The autocorrelation function was calculated using one-dimensional slices of the medium along each of the three orthogonal directions, with an average then computed across all three orientations. Similarly, the amplitude spectrum was derived from one-dimensional slices and subsequently averaged across directions.

The results of this analysis are presented in Figure S1. The analysis indicates that the properties of the resulting medium closely align with a Von Kármán distribution, with a parameter $k=2$

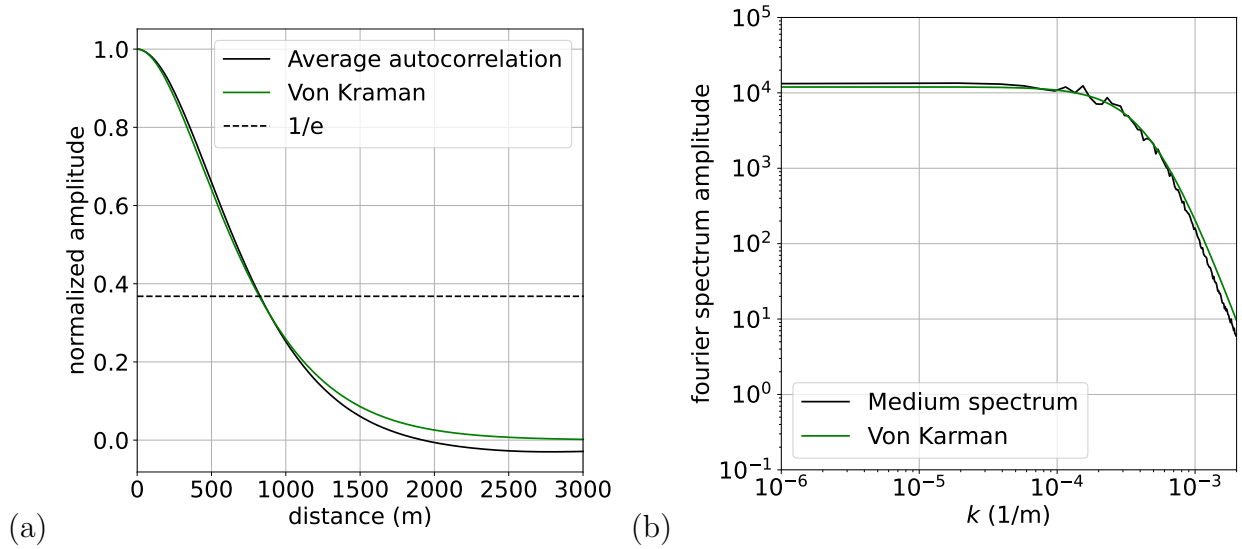


Figure S1. Autocorrelation of the medium (a) and its spectrum (b), fitted with a Von Kármán function, characterized by $k=2$ and a correlation length of 320 meters.

and a correlation length of 320 meters.

Consequently, the same parameters were used to solve the RTE.

Finally, the last aspect to consider is the boundary conditions at the edges of the medium in the elastic wave simulations. Any boundary condition will inherently affect the observed signal: absorbing boundaries lead to wave absorption, causing energy leakage from the medium and a corresponding loss of backscattered energy, while reflective boundaries, such as free surfaces, result in total energy reflection.

To accurately model the physics of an infinite medium, it is essential to create a propagation medium large enough so that S-waves do not have enough time to travel from the source to the boundary and then return to the receivers. This requires a medium of large size, which, in computational terms, makes this type of simulation highly resource-intensive and expensive.

Text S2. Mean free path computation

The computation of the mean free path, requires the analysis of the radial coherent field, which is obtained through spatial averaging of the radial component of displacement.

Table S1. Settings common to all the simulations of the Elastic Wave Equation.

	Parameter	Value
	Mesh size	52000x52000x52000 <i>m</i>
	Element size	200x200x200 <i>m</i>
	ABS sponge elements	14
	Free surface	None/Top
	Simulation time	12-24 <i>s</i>
	Sampling rate	833 <i>Hz</i>
	Moment tensor	$M_{zz} = M_{yy} = M_{xx} = 1$
	Source function peak	Gauss 3 <i>Hz</i>
Background medium	V_p	3000 <i>m/s</i>
	V_s	1744 <i>m/s</i>
	ρ	2400 <i>kg/m</i> ³
Heterogeneities	Correlation function	Von Kármán
	Correlation length	320 <i>m</i>

Under conditions of complete symmetry, as described in paragraph 2, once the receiver axes components are rotated towards the radial and transverse directions, the mean P field is obtained as follows:

$$\langle u_{rad}(t) \rangle = \sum_{i=0}^N u_{rad}(t)/N \quad (5)$$

Where $u_{rad}(t)$ is the radial component of the displacement and the sum is over the receivers located at the same distance from the source, r . The average value $\langle u_{rad}(t) \rangle$, is then corrected by the geometrical spreading:

$$\langle u_{corr}(t) \rangle = \langle u_{rad}(t) \rangle \cdot r \quad (6)$$

At this point, the amplitude Fourier spectrum is computed, $\langle \hat{u}_{corr}(t) \rangle$, and each individual component $\langle \hat{u}_{corr}(t) \rangle_i$ is considered. The fit is then performed considering the following expression:

$$\langle \hat{u}_{corr}(t) \rangle_i = a e^{-rc_i} \Leftrightarrow \log \langle \hat{u}_{corr}(t) \rangle_i = \ln a - rc_i \quad (7)$$

The mean free path is then obtained by linear regression for each frequency i , as $1/2c_i$.

Text S3. Diffusion constant computation

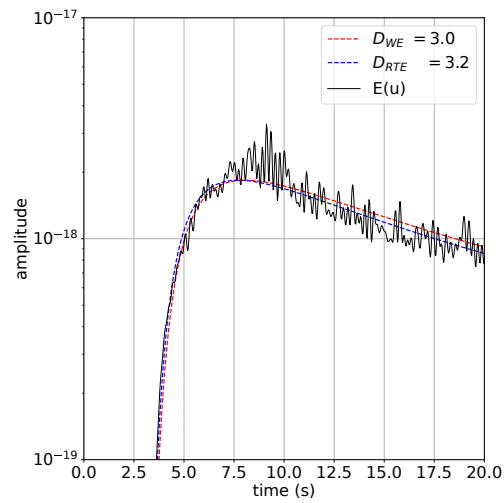


Figure S2. Energy evolution of the the displacement, observed in the full space 25% case at 10 km from the source . Comparison between the value obtained by solving the RTE (D_{RTE}) and the one obtained solving the Elastic Wave Equation (D_{WE}) fitting the diffusion equation 1

Text S4. Mean free times

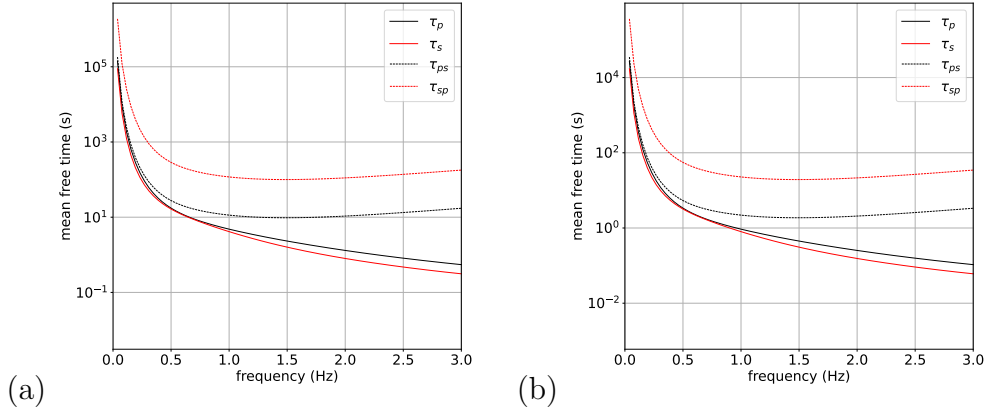


Figure S3. Mean free times for the two cases. τ_p and τ_s represent the average times that P or S seismic waves interact with a heterogeneity before being polarized into S or P modes, respectively. τ_{ps} and τ_{sp} are the average times after which, through interaction with a heterogeneity, P waves convert to S waves and S waves convert to P waves, respectively. In the case of $\epsilon = 25\%$, it can be observed that τ_p/v_p , above 3Hz, would become smaller than the correlation length. This is physically impossible and arises from the fact that the mean free time calculations were performed using the Born approximation, which becomes unreliable under strong scattering conditions at high frequencies.

Text S5. Two more case studies

In this section, we present two additional case studies. The first, shown in Figure S4, analyzes a full-space medium considering an isotropic moment tensor. The second, presented in Figure S5, examines a half-space medium with a source described by a moment tensor $M_{zz} = 1$.

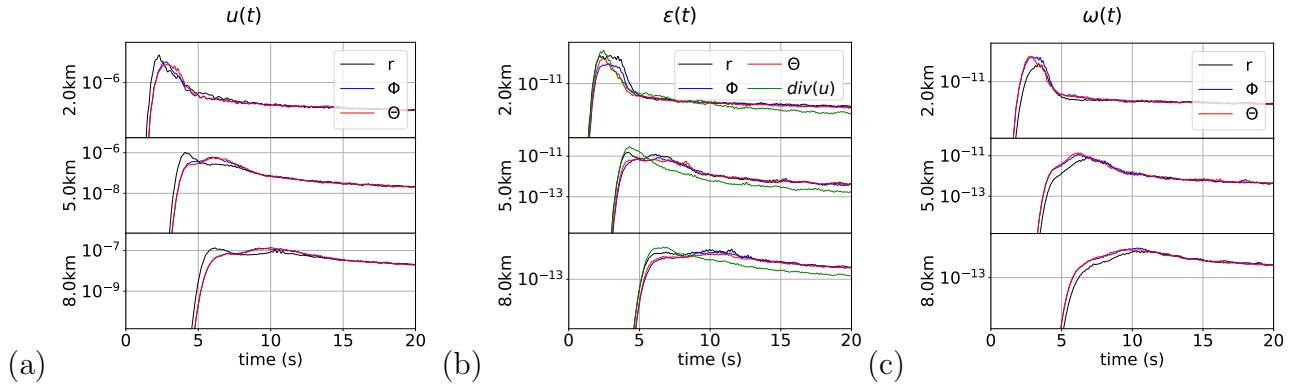


Figure S4. Case study in full space medium with $\epsilon = 17\%$ and isotropic moment tensor Comparison of the energy evolution of the radial and transverse components of the displacement (a), linear strain (b) and rotation (c).

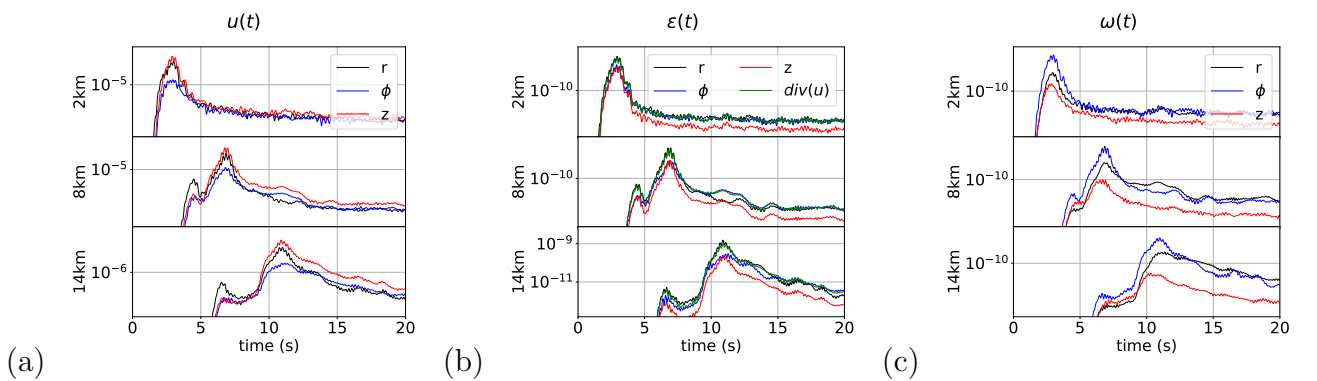


Figure S5. Case study in half space medium with $\epsilon = 10\%$ and $M_{zz} = 1$ Comparison of the energy evolution of the radial and transverse components of the displacement (a), linear strain (b) and rotation (c).

References

- Fornberg, B. (1987). The pseudospectral method: Comparisons with finite differences for the elastic wave equation. *GEOPHYSICS*, 52(4), 483-501. Retrieved from <https://doi.org/10.1190/1.1442319> doi: 10.1190/1.1442319
- Igel, H. (2017). *Computational seismology: A practical introduction*. Oxford, UK: Oxford University Press. Retrieved from <https://global.oup.com/academic/product/computational-seismology-9780198717409>
- Komatitsch, D. (1997). *Méthodes spectrales et éléments spectraux pour l'équation de l'élastodynamique 2d et 3d en milieu hétérogène* (Doctoral dissertation, Institut de Physique du Globe de Paris). Retrieved from <https://theses.hal.science/tel-00007568/>
- Margerin, L. (2005). Introduction to radiative transfer of seismic waves. In *Seismic earth: Array analysis of broadband seismograms* (p. 229-252). American Geophysical Union (AGU). Retrieved from <https://agupubs.onlinelibrary.wiley.com/doi/abs/10.1029/157GM14> doi: <https://doi.org/10.1029/157GM14>
- Margerin, L., Bajasas, A., & Campillo, M. (2019, 08). A scalar radiative transfer model including the coupling between surface and body waves. *Geophysical Journal International*, 219(2), 1092-1108. Retrieved from <https://doi.org/10.1093/gji/ggz348> doi: 10.1093/gji/ggz348
- Margerin, L., Campillo, M., & Van Tiggelen, B. (2000). Monte carlo simulation of multiple scattering of elastic waves. *Journal of Geophysical Research: Solid Earth*, 105(B4), 7873-7892. Retrieved from <https://agupubs.onlinelibrary.wiley.com/doi/abs/10.1029/1999JB900359> doi: <https://doi.org/10.1029/1999JB900359>
- Tregoures, N. P., & van Tiggelen, B. A. (2002). Quasi-two-dimensional transfer of elastic waves. *Physical Review E*, 66(3), 036601.